Available online at www.sciencedirect.com
SCIENCE DIRECT®
Bioorganic & Medicinal Chemistry 13 (2005) 5240–5252
Bioorganic & Medicinal Chemistry

Inhibition of the severe acute respiratory syndrome 3CL protease by peptidomimetic α,β-unsaturated esters

Jiun-Jie Shie,[a] Jim-Min Fang,[a,b,*] Tun-Hsun Kuo,[c] Chih-Jung Kuo,[c] Po-Huang Liang,[b,c,*] Hung-Jyun Huang,[a] Yin-Ta Wu,[b] Jia-Tsrong Jan,[d] Yih-Shyun E. Cheng[b] and Chi-Huey Wong[b]

[a]*Department of Chemistry, National Taiwan University, Taipei 106, Taiwan*
[b]*The Genomics Research Center, Academia Sinica, Taipei 115, Taiwan*
[c]*Institute of Biological Chemistry, Academia Sinica, Taipei 115, Taiwan*
[d]*Institute of Preventive Medicine, National Defense University, Taipei, Taiwan*

Received 28 April 2005; revised 26 May 2005; accepted 26 May 2005
Available online 1 July 2005

Dedicated to Professor Koji Nakanishi on the occasion of his 80th birthday and to honor him for receiving the 2004 Tetrahedron Prize.

Abstract—The proteolytic processing of polyproteins by the 3CL protease of severe acute respiratory syndrome coronavirus is essential for the viral propagation. A series of tripeptide α,β-unsaturated esters and ketomethylene isosteres, including AG7088, are synthesized and assayed to target the 3CL protease. Though AG7088 is inactive ($IC_{50} > 100$ μM), the ketomethylene isosteres and tripeptide α,β-unsaturated esters containing both P1 and P2 phenylalanine residues show modest inhibitory activity ($IC_{50} = 11$–39 μM). The Phe-Phe dipeptide inhibitors **18a**–**e** are designed on the basis of computer modeling of the enzyme–inhibitor complex. The most potent inhibitor **18c** with an inhibition constant of 0.52 μM is obtained by condensation of the Phe-Phe dipeptide α,β-unsaturated ester with 4-(dimethylamino)cinnamic acid. The cell-based assays also indicate that **18c** is a nontoxic anti-SARS agent with an EC_{50} value of 0.18 μM.

1. Introduction

Severe acute respiratory syndrome (SARS), which first occurred in Guandong (China) in November 2002, has spread over many countries in 2003. This illness is caused by infection with a novel human coronavirus (SARS-CoV).[1] The fatality rate of SARS-CoV infection is rather high, estimated to be 14–15%. In only a few months nearly 1000 lives were claimed.[2] The natural source of SARS-CoV is unclear, though studies on the molecular evolution of SARS-CoV indicate that the virus may have emerged from wild animals.[3] At present, no efficacious therapy for SARS is available. Therefore, a search for effective antivirals for the SARS-CoV is of current interest.

The SARS-CoV belongs to Coronaviridae family,[4] which includes porcine transmissible gastroenteritis virus (TGEV), human coronavirus (HCoV) 229E, mouse hepatitis virus, bovine coronavirus, and infectious bronchitis virus. The SARS-CoV is a positive-strand RNA virus that encodes two replicase polyproteins, pp1a and pp1b.[4] Extensive proteolytic processing of these nonstructural polyproteins is required to provide the functional proteins for viral propagation. These processes are mediated primarily by the main protease (M^{pro}), which is also known as dimeric chymotrypsin-like protease ($3CL^{pro}$).[5] The active site of SARS-CoV 3CL protease contains Cys145 and His41 to constitute a catalytic dyad, in which cysteine functions as the common nucleophile in the proteolytic process.[5] The 3CL protease cleaves pp1a at no less than 11 conserved sites with a sequence of (Leu, Met, Phe)-Gln ↓ (Ser, Ala, Gly), in which a P1 glutamine residue invariably occupies the S1 site.[5,6] The 3CL protease is essential for the propagation of the virus, and thus serves as a key target for the discovery of anti-SARS drugs.

Keywords: Severe acute respiratory syndrome; 3CL protease inhibitors; Peptides; α,β-Unsaturated esters; Cell-based assay; Antiviral agent.
* Corresponding authors. Tel.: +8862 23637812, fax: +8862 23636359 (J.-M.F.); e-mail: jmfang@ntu.edu.tw

0968-0896/$ - see front matter © 2005 Elsevier Ltd. All rights reserved.
doi:10.1016/j.bmc.2005.05.065

So far, only a few inhibitors have been validated by in vitro protease assays. These protease inhibitors include C_2 symmetric peptidomimetic compounds,[7] zinc-conjugated compounds,[8] bifunctional aryl boronic acids,[9] a quinolinecarboxylate derivative,[10] a thiophenecarboxylate,[11] and phthalhydrazide-substituted keto-glutamine analogs.[12]

AG7088, a ketomethyl isostere of a tripeptide-conjugated ester (compound **1a** in Scheme 1), is a potent inhibitor against human rhinovirus (HRV) 3C protease,[13] which is also a cysteine protease that mediates the maturation cleavages of replicase polyproteins.[14] The structure of AG7088 incorporates a γ-lactam moiety to mimic the amido side chain of the P1 glutamine residue. To improve the cell membrane permeability, the P2 phenylalanine residue is replaced by a methylene isostere bearing a 4-fluorophenyl substituent. The previous pharmacophore models,[5,15] by analogy to the structure of TGEV main proteinase, indicated that AG7088 can partially fit into the putative binding pocket of the SARS-CoV 3CL protease, and the moiety of conjugated ester in AG7088 may function as an acceptor of Cys145. Thus, AG7088 is proposed to be a model for the design of inhibitors against the SARS-CoV 3CL protease.

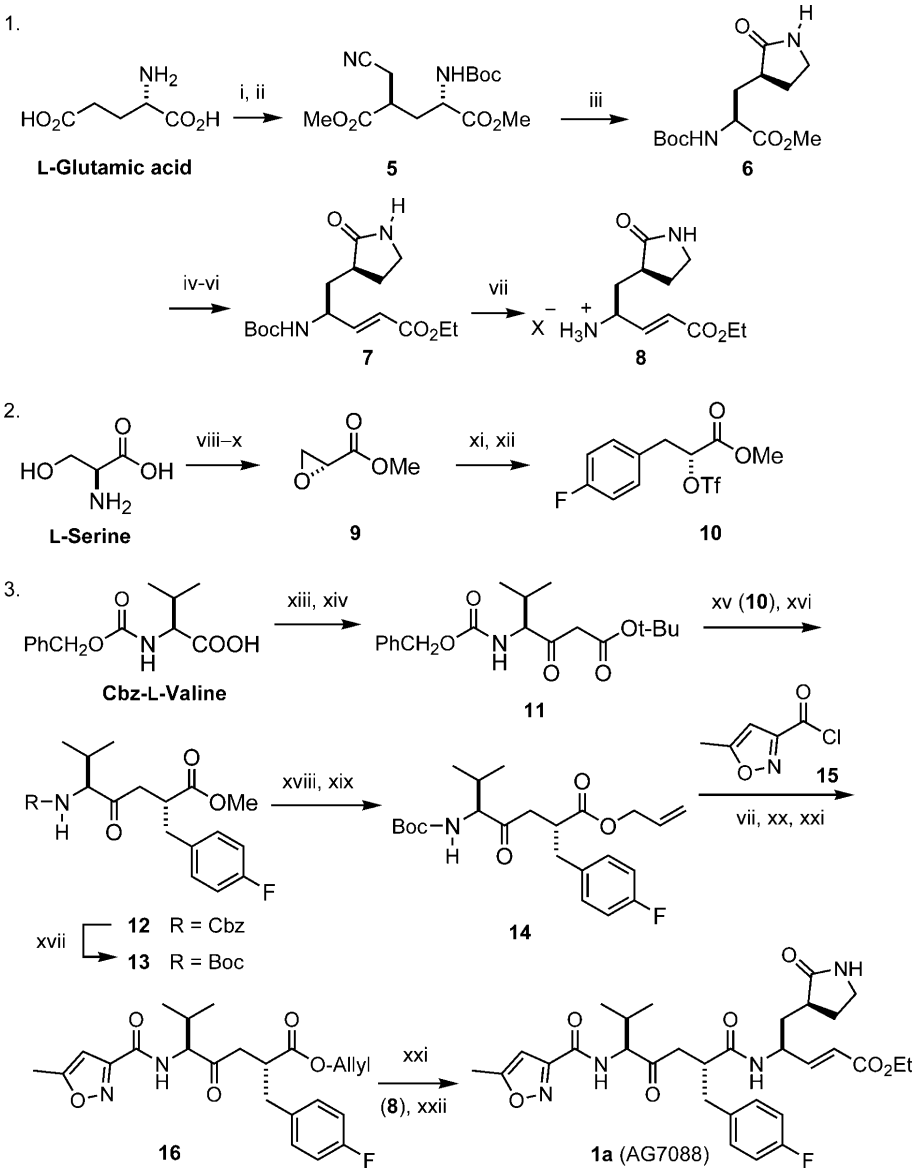

Scheme 1. Synthesis of AG7088. Reagents and conditions: (i) Me_3SiCl, MeOH, 0 °C, 18 h; then Boc_2O, Et_3N, 0–25 °C, 4 h; 96%. (ii) $LiN(SiMe_3)_2$, THF, −78 °C, 3 h; then $BrCH_2CN$, 3.5 h; 82%. (iii) H_2, cat. PtO_2, MeOH, $CHCl_3$, 25 °C, 12 h; then NaOAc, reflux, 12 h; 81%. (iv) $NaBH_4$, LiCl, THF, EtOH, 25 °C, 18 h; 89%. (v) Pyridine-SO_3, Me_2SO, CH_2Cl_2, Et_3N, −10 °C, 3 h. (vi) $[EtO_2CCHPO(OEt)_2]^-Na^+$, THF, −78 °C, 1 h; 75% yield for two steps. (vii) HCl, 1,4-dioxane, rt, 2 h. (viii) HBr, $NaNO_2$, KBr, H_2O, −10 °C, 12 h. (ix) KOH, EtOH, 0 °C, 12 h. (x) Me_2SO_4, CH_2Cl_2, $(PhCH_2)Et_3N^+Cl^-$, rt, 24 h; 70% for three steps, (xi) 4-FC_6H_4MgBr, CuBr–Me_2S, THF, −35 °C, 1 h; 86%. (xii) $(CF_3SO_2)_2O$, 2,6-lutidine, CH_2Cl_2, 0 °C, 40 min. (xiii) 1,1′-carbonyldiimidazole, THF, rt, 1 h. (xiv) CH_3CO_2-*t*-Bu, $LiN(i\text{-}Pr)_2$, THF, −78 °C, 1 h; 65%. (xv) NaH, THF, 0 °C, 30 min; then triflate **10**, THF, 0 °C to rt, 24 h. (xvi) CF_3CO_2H, CH_2Cl_2, rt, 24 h; 71% for two steps, (xvii) H_2, Pd/C, Boc_2O, MeOH, rt, 10 h; 83%. (xviii) LiOH (1.1 equiv), H_2O, 1 h, 0 °C; 90%. (xix) allyl iodide, Cs_2CO_3, DMF, 45 °C, 5 h; 85%. (xx) *N*-methylmorpholine (NMM), CH_2Cl_2, 0–25 °C, 2 h; 88%. (xxi) $Pd(PPh_3)_4$, morpholine, THF, 25 °C, 3 h; 85%. (xxii) HOBt, EDCI, NMM, DMF, 0–25 °C, 20 h; 70%.

In this paper, we describe the synthesis, the inhibition of SARS-CoV 3CL protease and anti-SARS activity of AG7088, the related ketomethylene isosteres and the peptidomimetic α,β-unsaturated esters. Although AG7088 turns out to be inactive, the α,β-unsaturated ester **18c** is found to be a potent antiviral agent with K_i of 0.52 μM and EC_{50} of 0.18 μM.

2. Results and discussion

2.1. Synthesis of AG7088 and the related compounds

On the basis of the previously reported methods,[13a,16] an improved synthesis of AG7088 was accomplished by using the natural glutamic acid, serine, and valine as the building blocks (Scheme 1). In this approach, the dianionic alkylation of *N*-Boc glutamic acid dimethyl ester (step ii) occurred in a highly stereoselective manner, giving **5** as the exclusive product (82% yield).[16b] Reduction of the cyano group in **5** by catalytic hydrogenation, followed by in situ cyclization, afforded γ-lactam **6** in 81% yield. The ester group in **6** was effectively reduced by $NaBH_4$ in the presence of LiCl. The alcohol product was then oxidized to an aldehyde (Parikh–Doering method), which was subsequently condensed with a Wittig reagent (Emmons method) to give the conjugated ester **7** in 75% yield (from **6**).

On the other hand, the epoxyester **9** with (*R*)-chirality was obtained from L-serine via diazotization, bromide substitution, and base treatment.[17] By the assistance of CuBr, the Grignard reagent 4-FC_6H_4MgBr reacted with **9** in a regioselective manner to give an alcohol product, which was then activated to the corresponding triflate **10**. The S_N2 reaction between triflate **10** and the valine-derived malonate **11** was followed by removal of the *tert*-butyloxycarbonyl (Boc) group under acidic conditions to provide the desired ketomethylene isostere **12**. Catalytic hydrogenation of **12** in the presence of di-*tert*-butyl carbonate furnished a direct conversion of the benzyloxycarbonyl (Cbz) group to the Boc group in **13**. Some ketomethylene isosteres are known to be susceptible to epimerization in alkaline conditions.[13a] In our case, hydrolysis of **13** was realized by using 1.1 equiv of LiOH (0 °C, 1 h), without complication of epimerization, and the acid product was then treated with allyl iodide in the presence of Cs_2CO_3 to give the allyl ester **14** as a single product. An oxidative condensation of 2,5-hexadione with aqueous HNO_3 gave 5-methyl-3-isoxazolecarboxylic acid,[18] and the corresponding acyl chloride **15** reacted with **14**, after removal of the Boc group, to give amide **16** in the presence of *N*-methylmorpholine. The allyl group in **16** was smoothly removed by the catalysis of $Pd(PPh_3)_4$, and the resulting acid was coupled with the amine derived from **7** to culminate in the synthesis of AG7088. The spectroscopic properties of our prepared sample are in agreement with those reported for AG7088.[13]

For the investigation of the structure–activity relationship, we also applied a combinatorial approach to synthesize other ketomethylene isosteres (e.g., **1b–d**) having various R and R′ substituents at the P2 and N-terminal sites. In addition, the corresponding tripeptidomimetic α,β-unsaturated esters **2a–d** were prepared by the procedures generally used in peptide synthesis. By using phenylalanine to replace the P1 residue of lactam-glutamate, a series of ketomethylene isosteres **3a–d** and tripeptidomimetic α,β-unsaturated esters **4a–d** were also synthesized for comparison study.

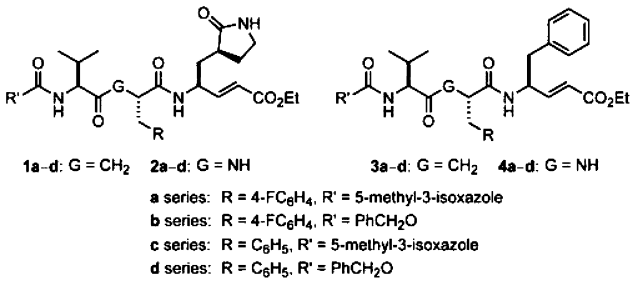

2.2. Inhibition assay against the SARS-CoV 3CL protease

According to the previously described fluorometric method,[7,19] the conjugated esters of **1–4** series were subjected to the inhibition assay against the SARS-CoV 3CL protease. The initial velocities of the inhibited reactions using 50 nM of SARS-CoV 3CL protease and 6 μM of the fluorogenic substrate were plotted against the different inhibitor concentrations to obtain the IC_{50} values. In comparison (Table 1), most of the tripeptidomimetic α,β-unsaturated esters (**2** and **4** series) tend to be more active than the corresponding ketomethylene isosteres (**1** and **3** series).

Although AG7088 has been predicted to be a good inhibitor of SARS 3CL protease,[5,15] it turned out to be inactive at a concentration of 100 μM in our enzymatic assay. This result is in agreement with a cell-based assay that indicates AG7088 is inactive to the SARS-

Table 1. IC_{50} values of AG7088 (**1a**) and the related compounds for inhibition of SARS-CoV 3CL protease[21]

Compound	G	R	R′	IC_{50} (μM)[a]
1a	CH_2	4-FC_6H_4	5-Me-isoxazol-3-yl	>100
1b	CH_2	4-FC_6H_4	$PhCH_2O$	>100
1c	CH_2	Ph	5-Me-isoxazol-3-yl	>100
1d	CH_2	Ph	$PhCH_2O$	>100
2a	NH	4-FC_6H_4	5-Me-isoxazol-3-yl	>100
2b	NH	4-FC_6H_4	$PhCH_2O$	>100
2c	NH	Ph	5-Me-isoxazol-3-yl	80
2d	NH	Ph	$PhCH_2O$	85
3a	CH_2	4-FC_6H_4	5-Me-isoxazol-3-yl	39
3b	CH_2	4-FC_6H_4	$PhCH_2O$	31
3c	CH_2	Ph	5-Me-isoxazol-3-yl	13
3d	CH_2	Ph	$PhCH_2O$	38
4a	NH	4-FC_6H_4	5-Me-isoxazol-3-yl	21
4b	NH	4-FC_6H_4	$PhCH_2O$	11
4c	NH	Ph	5-Me-isoxazol-3-yl	30
4d	NH	Ph	$PhCH_2O$	11

[a] The highest concentration of samples used in tha assays is 100 μM.

CoV.[7,20] However, the structure–activity relationship study on AG7088 analogs indicated that the inhibitory activity was improved by replacing the lactam-glutamine isostere with L-phenylalanine. For example, compounds **3a**–**d** and **4a**–**d** with a phenyl group replacing the P1 lactam moiety showed better inhibitory activity (IC_{50} = 11–39 μM) than AG7088 (**1a**) and its analogs (**lb**–**d** and **2a**–**d**; $IC_{50} \geqslant 80$ μM).

2.3. Molecular modeling for the enzyme–inhibitor complexes

The observation of enhanced inhibitory activities of the compounds with phenylalanine replacement at the P1 positions prompted us to conduct the computational modeling of the enzyme in complexation with AG7088 or the inhibitor **3c**. The target structure used for modeling is deduced from the complex structure of the SARS-CoV 3CL protease mutant (C145A) and the hexapeptide substrate, Ser-Gly-Val-Thr-Phe-Gln.[21] Accordingly, the apoenzyme B-chain containing Cys145 was applied in the molecular simulation with the designated inhibitor.

From the computer docking, AG7088 cannot bind properly to the active site of SARS-CoV 3CL protease (Fig. 1). Though AG7088 can position its P2 fluorophenyl side chain into the S2 site, its P1 lactam moiety cannot fit to the S1 site of the protease without interfering with the proper disposition of the terminal conjugated ester group in the S1′ site. Unlike the effective binding of AG7088 with the Thr142 of Rhinovirus 3CL protease,[5] the conjugated ester in AG7088 is prevented from suitable interaction with the Asn142 of the SARS-CoV

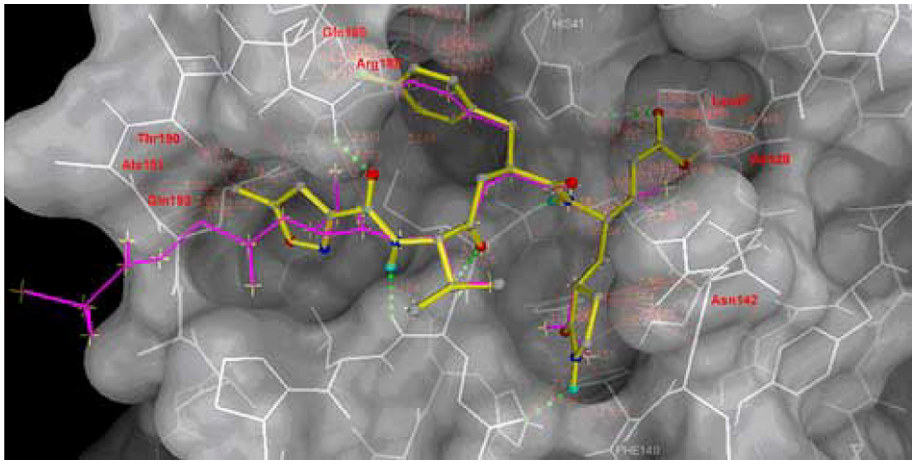

Figure 1. Structure of AG7088 (yellow) is modeled into structure of SARS-CoV $3CL^{pro}$ by superimposing on the cocrystal structure of hexapeptide Ser-Gly-Val-Thr-Phe-Gln (magenta, the P6–P1 fragment). The close contact distances are computed in MGLTOOLS with a van der Waals radius factor of 1.0. Those residues that can contribute major steric effects ($d < 2.0$ Å) to AG7088 model are labeled in red.

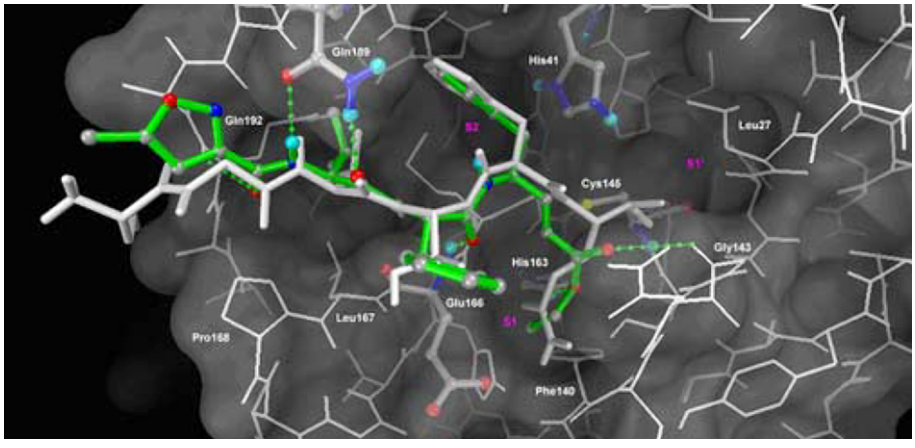

Figure 2. A modeled complex of SARS-CoV 3CL protease with the inhibitor **3c**. The protease is shown in white line model, whereas the catalytic dyad (His41 and Cys145), His163 in S1 site, Glu166, Gln189 and compound **3c** are highlighted in atom-colored ball-and-stick model. The stick of compound **3c** is colored green. Individual atoms are displayed in gray (carbon), blue (nitrogen), red (oxygen), and yellow (sulfur). The hexapeptide Ser-Gly-Val-Thr-Phe-Gln (P6-P1), in white stick model, is overlaid for a comparison. The displayed structure of compound **3c** is elected from the docked cluster with the lowest binding free energy. Potential hydrogen-bonding interactions of compound **3c** with residues in the binding pocket are shown in green broken lines.

3CL protease, thereby forcing it to adopt a position outside the pocket defined by Cys145, Thr25, and Leu27. The possible steric effects are also exerted by the fluorophenyl group against Arg188 in the S2 pocket and by the isoxazoyl moiety against the hydrophobic residues in the S4 pocket.

In contrast, compound **3c** having two phenyl groups at the P1 and P2 residues can fit, respectively, in the S2 and S3 pockets of the SARS-CoV 3CL protease (Fig. 2). The overlay of Ser-Gly-Val-Thr-Phe-Gln hexapeptide upon **3c** shows a conformational similarity. The simulation model also reveals the key hydrogen bondings of **3c** with the Glu166, Gln189, and Gln192 residues in the active sites of protease. It is noted that the isoxazolyl moiety in **3c** adopts a conformation different from that in AG7088, and thus accommodates a favorable hydrogen bonding with Gin 192 in the S4 pocket. The binding mode of **3c** thus contributes to a better inhibitory activity ($IC_{50} = 13\ \mu M$) than that of AG7088 ($IC_{50} > 100\ \mu M$). As the P1 and P2 residues in **3c** move to the S2 and S3 pockets, the moiety of conjugated ester in **3c** may occupy the S1 site to exert interactions with His 163 and Gly143. However, the conjugated ester is still unreachable (>4.5 Å) by Cys145 to render a Michael reaction for the covalent C–S bond formation.

2.4. Design of dipeptide inhibitors having double Michael acceptors at both C- and N-terminals

As the molecular modeling reveals that compounds of **3** and **4** series show better inhibitory activity than the compounds of **1** and **2** series by placing their P1 and P2 phenylalanine residues in the S2 and S3 pockets of the SARS-CoV 3CL protease. We surmise that the Phe-Phe dipeptides containing conjugated amido moieties at the N-terminals, such as compounds **18a–e** with virtually pseudo-C_2 symmetry, may exhibit greater inhibitory activities.

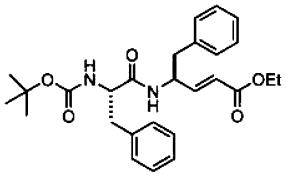

17

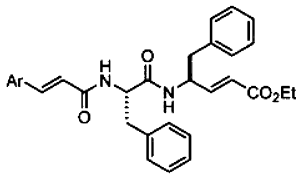

18a Ar = 4-PhC_6H_4
18b Ar = 4-$O_2NC_6H_4$
18c Ar = 4-$Me_2NC_6H_4$
18d Ar = 2,4-$(MeO)_2C_6H_3$
18e Ar = 3,4-$(OCH_2O)C_6H_3$

A strategy of parallel synthesis in a microtiter plate[22] is applied for the construction of **18a–e** and analogs. Thus, the Phe-Phe dipeptidyl α,β-unsaturated ester **17** was prepared by the amidation of *N*-Boc-phenylalanine with ethyl 4-amino-5-phenyl-2-pentenoate,[23] and then treated with HCl in 1,4-dioxane to remove the Boc group. The resulting amine was reacted with a library of α,β-unsaturated carboxylic acids to give **18a–e** and analogs, which were subjected, without isolation, to the inhibition assay against the SARS-CoV 3CL protease. On the basis of the preliminary results of assays, some of the most promising inhibitor candidates (**18a–e**) were selected for the scale-up synthesis. The IC_{50} values and inhibition constants (K_i) of the pure samples were then measured to validate their activities (Table 2).

It is fortunate to find that the dipeptidomimetic α,β-unsaturated esters **18a–e** bearing the cinnamyl moieties at the N-terminals showed good inhibitory activity against the SARS-CoV 3CL protease. Among them, compound **18c** (JMF1521) derived from Phe-Phe dipeptide α,β-unsaturated ester and 4-(dimethylamino)cinnamic acid is the most potent inhibitor with an IC_{50} value of 1 μM and K_i value of 0.52 μM. The double reciprocal plots of the initial rate versus substrate concentration indicate that all these compounds (**18a–e**) are competitive inhibitors. A representative example for the inhibition of the SARS-CoV 3CL protease by **18c** is shown in Figure 3.

The computer model for the complex of SARS-CoV 3CL protease with **18c** (Fig. 4) shows that the P1 and P2 phenyl groups occupy the S2 and S3 pockets, respectively. The conjugated (dimethylamino)cinnamyl group disposes a rather rigid coplanar structure in the N-terminal and renders effective hydrogen bondings with the Glu166, Gln189, and Gln192 residues of the enzyme.

For comparison, compounds **19**, **20**, and **21a–c** were also synthesized and subjected to the inhibition assay.

Table 2. Protease inhibition, anti-SARS, and cytotoxicity properties of the dipeptide inhibitors **18a–e**

Compound	IC_{50} (μM)[a]	K_i (μM)	EC_{50} (μM)	CC_{50} (μM)[b]	S.I.[c]
1a	>100	ND[d]	—[e]	ND	
3c	13	ND[d]	—[e]	ND	
18a	10	6.44 ± 0.8	18.86	>200	>10
18b	5	2.48 ± 0.89	9.45	>200	>20
18c	1	0.52 ± 0.024	0.18	>200	>1000
18d	10	9.049 ± 2.35	0.11	>200	>1000
18e	7	3.046 ± 0.61	0.16	>200	>1000

[a] The highest concentration of samples is 10 μM in the assay against the SARS-CoV 3CL protease.
[b] The highest concentration of sample is 200 μM in the assay of cytotoxicity on Vero E6 cells.
[c] Selectivity index, the ratio of CC_{50} to EC_{50}.
[d] Not determined.
[e] No protective effect against infection of Vero E6 cells at the concentration of 10 μM.

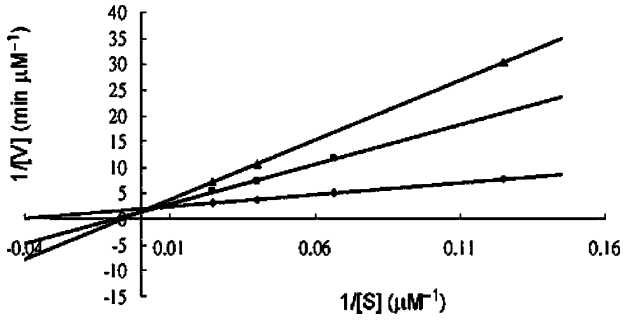

Figure 3. Lineweaver–Burk plot for inhibition of the SARS-CoV 3CL protease by the dipeptide-conjugated ester **18c**.

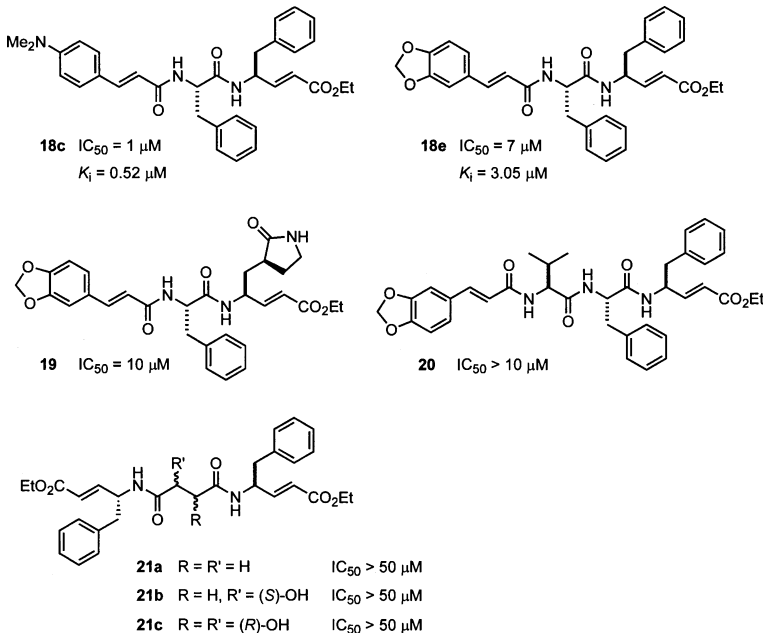

The dipeptide derivative **19** contains a γ-lactam moiety at the P1 site in lieu of the phenyl group in **18e**. The tripeptide derivative **20** is a homolog of dipeptide **18e** by the introduction of an additional P3 valine residue. The dimeric peptide conjugated esters **21a**–**c** were prepared by using a diacid, e.g., succinic acid, *S*-malic acid, and (2*R*,3*R*)-tartaric acid, as the core structure to link with the phenylalanine α,β-unsaturated ester. Compound **18e** derived from Phe-Phe dipeptide and 3,4-(methylenedioxy)cinnamic acid showed an IC_{50} value of 7 μM and K_i value of 3.05 μM. The assays indicated that none of **19**, **20**, and **21a**–**c** were active against the SARS-CoV 3CL protease

2.5. Cell-based assays

The antiviral activities of **1a** (AG7088), **3c**, and **18a**–**e** were evaluated by the protection from cytopathogenic effect (CPE) on Vero E6 cells.[7] While **1a** and **3c** are inactive, **18a** is active as an anti-SARS agent at a concentration of 3.3 μM, and **18b**–**e** are even more potent with anti-SARS activities at 1 μM. The anti-SARS compounds **18a**–**e** were further evaluated at multiple concentrations to deduce the concentrations for 50% inhibition of the host growth (CC_{50})[24] and the 50% inhibitory concentrations of virus replication (EC_{50}) by the enzyme-linked immunosorbent assay (ELISA).[7] None of **18a**–**e** are toxic to the growth of host cells at 200 μM, the highest concentration used in this assay. The EC_{50} values of compounds **18c**, **18d**, and **18e** deduced by ELISA measurements of the viral spike protein expressions are 0.11–0.18 μM (Table 2). Thus, the ratio of CC_{50} to EC_{50}, the selectivity index (SI), for compounds **18c**–**e** is very high (>1000). The antiviral activity of **18c** was confirmed by Western blotting assay using antispike protein monoclonal antibody (Fig. 5). A significant suppression of viral expression of 3CL protease was also observed on treatment with **18c** at a concentration of 1 μM (data not shown).

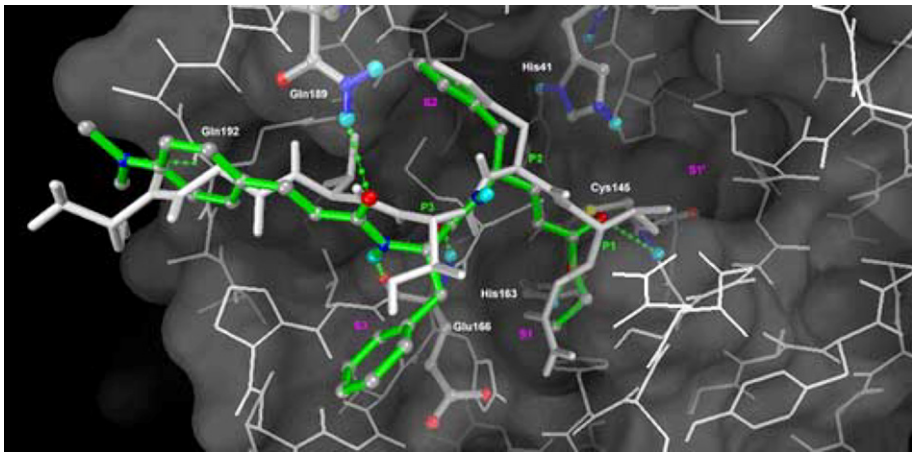

Figure 4. A modeling complex of SARS-CoV 3CL protease with the inhibitor **18c** (colored green). The notations are the same as those shown in Figure 2.

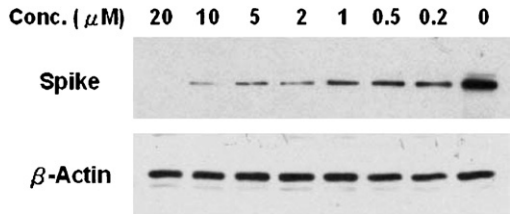

Figure 5. Western blot analysis of the inhibitory effect of compound **18c** on the SARS-CoV spike protein synthesis.

Although the real reasons for smaller EC_{50} than K_i are unclear, we speculate that the environment and the physical state of the 3CL protease may be very different between the SARS-infected cells and the recombinant 3CL protease used in the cell-free assays. We tried assay conditions using a low concentration (5 nM) of the SARS 3CL protease in an extended reaction time (1 h) and showed no sign of slow inhibition due to the irreversible bond formation with compounds **18c**–**e**. The assay with a prolonged period is infeasible due to depletion of the substrate. It is uncertain whether the actual inhibitor binding may be tighter through a slow conformational change. On the other hand, the inhibitor may partially block the process for polyprotein maturation.[21] Previous studies suggested that dimeric 3CL protease is the active form.[5] Studies using cell-free systems also suggested that the N- and C-terminal tagged forms can be autoproteolyzed, and the autoproteolytic process is susceptible to protease inhibitors.[21] Furthermore, 3CL protease can also proteolyze polyproteins in trans for their maturation.[21] The cell-free studies therefore suggested the presence of multiple forms of proteolytic activities, and the physical states of the 3CL protease and their reactivity in SARS-infected cells are likely to be even more complicated. Like 3CL protease, the HIV protease is synthesized as part of the polyprotein that is autoproteolyzed for the protease maturation. It is thought that the dimerization of the HIV protease takes place while the enzyme is still in the form of a polyprotein that is synthesized and migrated to the membrane budding sites. Both the location and the timing of the autoproteolysis are crucial for the HIV viral infectivity.[25,26] Very little is known on the physical state and the enzyme reactivity of the 3CL protease in SARS-infected cells. It is thus impossible to surmise, at this time, the rate-limiting target of the protease inhibitors on SARS infectivity. More studies are needed to understand the regulation, proteolytic activity, and physical states of the enzyme present in the SARS-infected cells for the control of SARS virus using protease inhibitors.

3. Conclusion

We have devised an improved method for the preparation of AG7088 in an efficient manner. Although AG7088 and the analogs bearing P1 lactam-glutamine residue (**1a**–**d** and **2a**–**d**) show no inhibitory activity against the SARS-CoV 3CL protease, the related conjugated esters **3a**–**d** and **4a**–**d** are found to exhibit improved activities. The Phe-Phe dipeptide inhibitors **18a**–**e** are designed on the basis of computer modeling of the enzyme–inhibitor complex. The most potent inhibitor **18c**, with an inhibition constant of 0.52 μM, is obtained by condensation of the Phe-Phe dipeptide α,β-unsaturated ester with 4-(dimethylamino)cinnamic acid. The cell-based assays indicate that **18c** is a nontoxic anti-SARS agent with an EC_{50} value of 0.18 μM. In addition to valinomycin with an EC_{50} of 0.85 μM,[7] to our knowledge compounds **18c**–**e** represent the most potent anti-SARS agents known to date. Our computational study of structure–activity relationships shows that hydrogen bonding with the main chain Glu166 and the side chain Gln189 are crucial to the inhibitory potency. This interaction is supported by a modeling complex of SARS-CoV 3CL protease with the inhibitor **18c**. We are currently investigating the cocrystal structure, which can give an insight into the proposed complexation mode for further design of new anti-SARS compounds.

4. Experimental

4.1. General

Melting points are uncorrected. ^{1}H NMR spectra were recorded at 400 MHz; ^{13}C NMR spectra were recorded at 100 MHz. Chemical shifts (δ) are given in parts per million (ppm) relative to residual solvent [δ 7.24 (s) for $CHCl_3$ and δ 2.49 (m) for DMSO-d_6]. The splitting patterns are reported as s (singlet), d (doublet), t (triplet), and multiplet (m). Chemical shifts of ^{13}C NMR spectra are reported relative to $CDCl_3$ (δ 77.0 for the central line of triplet) and DMSO-d_6 [δ 39.5 (m)]. Mass spectra were recorded at an ionizing voltage of 70 or 20 eV. Merck silica gel 60F sheets were used for analytical thin-layer chromatography (TLC). Merck silica gel 60F glass plates (20 cm × 20 cm with 2 mm thickness) were used for preparative TLC. Column chromatography was performed on silica gel (70–230 mesh) using gradients of EtOAc/hexane as eluents.

4.2. Chemistry

Reactions requiring dry conditions were carried out under an inert atmosphere using standard techniques. All the reagents and solvents were of reagent grade and were used without further purification unless otherwise specified. THF was distilled from sodium benzophenone ketyl under N_2. Tripeptide ketomethylene isosteres **lb**–**d** and **3a**–**d** were prepared by the procedure similar to that for **1a** (AG7088). Peptide α,β-unsaturated esters **2a**–**d** and **4a**–**d** were prepared by the similar procedure. Compounds **5**–**13** were prepared according to the previously described procedures.[13a,16]

4.2.1. Allyl (2*R*,5*S*)-5-(*tert*-butoxycarbonyl)amino-2-(4-fluorobenzyl)-6-methyl-4-oxo-heptanoate (14). Lithium hydroxide (3.3 mmol, 3.3 mL of 1 M aqueous solution) was added to a solution of methyl ester **13** (1.186 g, 3 mmol) in MeOH (20 mL) at 0 °C. The mixture was stirred for 1 h at 0 °C, 1 N HCl (20 mL) was added,

and the mixture was extracted with EtOAc (30 mL, 4×). The combined organic layers were dried over $MgSO_4$ and concentrated under reduced pressure to provide a crude carboxylic acid (1.028 g, 90%).

The crude product was dissolved in DMF (20 mL) and treated with allyl iodide (0.36 mL, 4.0 mmol) in the presence of Cs_2CO_3 (1.14 g, 3.5 mmol) at 45 °C for 5 h. The mixture was diluted with water (20 mL) and extracted with EtOAc (30 mL, 3×). The combined organic layers were washed with water (20 mL, 3×), dried over Na_2SO_4, and concentrated under reduced pressure. The residue was purified by flash column chromatography (EtOAc/hexane, 1:1) to afford allyl ester **14** (839 mg, 84%) as a colorless oil.

Compound **14**: oil; TLC (EtOAc/hexane, 1:1) $R_f = 0.33$; IR (neat) 3101, 2983, 1721, 1605, 1451, 1111 cm^{-1}; ^1H NMR ($CDCl_3$, 400 MHz): δ 7.15–7.12 (2H, m), 7.02–6.90 (2H, m), 5.85–5.69 (1H, m), 5.27–5.19 (2H, m), 5.10 (1H, d, $J = 8.6$ Hz), 4.53–4.49 (2H, m), 4.25–4.13 (1H, m), 3.16–3.10 (1H, m), 3.08–2.95 (1H, m), 2.91–2.69 (2H, m), 2.55–2.38 (1H, m), 2.17–2.00 (1H, m), 1.49 (9H, s), 0.93 (3H, d, $J = 6.8$ Hz), 0.70 (3 H, d, $J = 6.8$ Hz); ^{13}C NMR ($CDCl_3$, 100 MHz): δ 204.4 (C), 171.1 (C), 148.5 (C), 137.6 (C), 135.0 (CH), 129.1 (CH, 2×), 128.8 (CH, 2×), 126.6 (C), 114.1 (CH_2), 71.8 (CH_2), 63.1 (C), 42.5 (CH), 38.9 (CH_2), 32.7 (CH_2), 28.1 (CH), 28.0 (CH_3, 3×), 19.7 (CH), 16.3 (CH_3, 2×); FAB-MS 422.2 (M^++H); HRMS calcd for $C_{23}H_{33}FNO_5$ (M^++H), 422.2343; found, 422.2341.

4.2.2. Allyl (2*R*,5*S*)-2-(4-fluorobenzyl)-6-methyl-5-[(5-methyl-3-isoxazolyl)carbonyl)]amino-4-oxoheptanoate (16). A solution of HCl in 1,4-dioxane (4.0 M, 5 mL) was added to a solution of allyl ester **14** (210 mg, 0.5 mmol) in 1,4-dioxane (5 mL) at room temperature. The mixture was stirred for 2 h, and then concentrated under reduced pressure to give a crude aminium salt. This material was dissolved in CH_2Cl_2 (10 mL) and cooled to 0 °C. 4-Methylmorpholine (0.17 mL, 1.5 mmol) and 5-methylisoxazole-3-carbonyl chloride (88 mg, 0.6 mmol) were added sequentially. The mixture was removed from the ice bath, stirred for 2 h at 25 °C, and diluted with CH_2Cl_2 (20 mL). The mixture was washed with 10% aqueous citric acid (20 mL) and brine (20 mL). The organic phase was dried over Na_2SO_4, concentrated, and purified by flash column chromatography (EtOAc/hexane, 1:4) to give the desired product **16** (187 mg, 88%).

Compound **16**: oil; TLC (EtOAc/hexane, 1:1) $R_f = 0.28$; IR (neat) 3071, 2944, 1714, 1700, 1612, 1466 cm^{-1}; ^1H NMR ($CDCl_3$, 400 MHz): δ 7.13–7.09 (2H, m), 6.98–6.87 (2H, m), 6.44 (1H, s), 5.86–5.61 (1H, m), 5.23–5.09 (3H, m), 4.61–4.52 (2H, m), 4.23 (1H, dd, $J = 8.5$, 3.7 Hz), 3.13–3.07 (1H, m), 2.97–2.86 (2H, m), 2.72–2.61 (1H, m), 2.51–2.40 (1H, m), 2.49 (3H, s), 2.21–2.03 (1H, m), 0.95 (3H, d, $J = 8.1$ Hz), 0.71 (3H, d, $J = 8.1$ Hz); ^{13}C NMR ($CDCl_3$, 100 MHz): δ 204.4 (C), 171.9 (C), 169.8 (C), 160.8 (C), 160.2 (C), 157.9 (C), 138.1 (C), 128.5 (CH, 2×), 128.2 (CH, 2×), 126.1 (CH), 112.1 (CH_2), 103.8 (CH), 72.6 (CH_2), 64.5 (CH), 39.0 (CH_2), 34.5 (CH_2), 28.6 (CH), 20.9 (CH), 20.3 (CH_3), 16.6 (CH_3, 2×); FAB-MS *m*/*z* 431.2 (M^++H); HRMS calcd for $C_{23}H_{28}FN_2O_5$ (M^++H), 431.1982; found, 431.1983.

4.2.3. Ethyl 4-[2-(4-fluorobenzyl)-6-methyl-5-(5-methyl-3-isoxazolyl)carbonylamino-1,4-dioxoheptylamino]-5-(2-oxo-3-pyrrolidinyl)-2-pentenoate (1a, AG7088). Compound **16** (129 mg, 0.3 mmol) in anhydrous THF (10 mL) was stirred with $Pd(PPh_3)_4$ (36 mg, 0.03 mmol) and morpholine (0.25 mL, 3.0 mmol) for 3 h at 25 °C. The mixture was concentrated under reduced pressure, diluted with CH_2Cl_2 (30 mL), and washed with 2 N HCl (10 mL) and water (20 mL). The organic phase was extracted with saturated $NaHCO_3$ aqueous solution (30 mL, 3×). The combined aqueous extracts were acidified to pH 2 with 5% aqueous $KHSO_4$ at 0 °C, and then extracted with Et_2O (30 mL, 5×). The ethereal extract was dried ($MgSO_4$), filtered, and the filtrate was concentrated under reduced pressure to give the corresponding acid of **16** (99 mg, 85%).

Compound **7** (81 mg, 0.25 mmol) was treated with HCl in 1,4-dioxane, by a procedure similar to that for **14**, to give aminium salt **8**. This material and the carboxylic acid derived from **16** (99 mg, 0.25 mmol) were dissolved in DMF (5 mL) and cooled to 0 °C, followed by the addition of 4-methylmorpholine (0.08 mL, 0.75 mmol), HOBt (41 mg, 0.3 mmol), and EDCI (58 mg, 0.3 mmol). The mixture was removed from the ice bath, stirred for 20 h at 25 °C, diluted with CH_2Cl_2 (15 mL), and washed with 10% aqueous citric acid (8 mL) and water (10 mL, 3×). The organic phase was dried over Na_2SO_4, concentrated, and purified by flash column chromatography ($MeOH/CH_2Cl_2$, 1:99) to provide 105 mg of **1a** (70% yield).

Compound **1a**: white solid; mp 180–182 °C (lit.[13a] mp 178–181 °C); TLC (CH_3OH/CH_2Cl_2, 1:9) $R_f = 0.50$; IR (KBr) 3299, 1678, 1521, 1325, 1180 cm^{-1}; ^1H NMR ($CDCl_3$, 400 MHz): δ 7.34 (1H, d, $J = 8.7$ Hz), 7.11–7.08 (2H, m), 6.94–6.90 (2H, m), 6.58 (1H, dd, $J = 11.7$, 5.2 Hz), 6.38 (1H, s), 6.05 (1H, br s, NH), 5.42 (1H, dd, $J = 11.6$, 1.4 Hz), 4.63 (1H, dd, $J = 8.7$, 4.4 Hz), 4.50–4.37 (1H, m), 4.14 (2H, q, $J = 6.8$ Hz), 3.31–3.20 (2H, m), 3.05–2.99 (1H, m), 2.98–2.89 (1H, m), 2.88–2.79 (1H, m), 2.70–2.51 (3H, m), 2.45 (3H, s), 2.25–2.00 (3H, m), 1.85–1.75 (1H, m), 1.74–1.60 (1H, m), 1.50–1.42 (1H, m), 1.25 (3H, t, $J = 6.8$ Hz), 0.85 (3H, d, $J = 6.8$ Hz), 0.79 (3H, d, $J = 6.8$ Hz) ; ^{13}C NMR ($CDCl_3$, 100 MHz): δ 206.7 (C), 173.4 (C), 171.1 (C), 166.0 (C), 162.6 (C), 160.2 (C), 158.9 (C), 158.1 (C), 147.1 (CH), 134.0 (C), 130.3 (CH, 2×), 120.5 (CH), 115.1 (CH), 114.8 (CH, 2×), 101.3 (CH), 62.8 (CH), 60.4 (CH_2), 49.0 (CH), 43.9 (CH), 42.0 (CH_2), 40.5 (CH_2), 38.3 (CH_2), 34.9 (CH_2), 30.4 (CH), 28.7 (CH_2), 19.9 (CH_3), 17.1 (CH_3), 14.3 (CH_2), 12.4 (CH_3); FAB-MS 599.3 (M^++H); HRMS calcd for $C_{31}H_{40}FN_4O_7$, 599.2801 (M^++H); found, 599.2811. Anal. calcd for $C_{31}H_{39}FN_4O_7$: C 62.19, H 6.57, N 9.36. Found: C 62.12, H 6.60, N 9.37.

4.2.4. Ethyl 4-(*tert*-butoxycarbonyl)amino-5-phenyl-2-pentenoate (17). Ethyl (2*E*,4*S*)-4-(*tert*-butoxycarbon-

yl)amino-5-phenyl-2-pentenoate[23] was prepared from *N*-Boc-L-Phe by a sequence of esterification (CH_3I, $KHCO_3$, rt, 8 h, 94%), reduction ($NaBH_4$, LiCl, THF, EtOH, rt, 12 h, 89%), oxidation (pyridine·SO_3, DMSO, Et_3N, −10 °C to rt, 1 h), and olefination [$EtO_2CCH_2PO(OEt)_2$, $NaN(TMS)_2$, THF, −78 °C to rt, 2 h, 84% for two steps], and then treated with HCl in 1,4-dioxane to remove the Boc group. The resulting amine was reacted with *N*-Boc-L-Phe in the presence of EDCI, HOBt, and 4-methylmorpholine, by a procedure similar to that for compound **1a**, to give the desired product **17** in 82% overall yield.

Compound **17**: white solid; mp 129–131 °C; TLC (EtOAc/hexane, 3:7) $R_f = 0.27$; IR (KBr) 3214, 1711, 1645 cm^{-1}; ^1H NMR ($CDCl_3$, 400 MHz): δ 7.30–7.15 (8H, m), 7.05 (2H, d, $J = 6.7$ Hz), 6.77 (1H, dd, $J = 15.5$, 4.3 Hz), 6.00 (1H, d, $J = 8.1$ Hz), 5.59 (1H, d, $J = 15.5$ Hz), 4.99–4.87 (2H, m), 4.29–4.25 (1H, m), 4.16 (2H, q, $J = 7.1$ Hz), 2.99–2.97 (2H, m), 2.81 (2H, d, $J = 6.7$ Hz), 1.40 (9H, s), 1.27 (3H, t, $J = 7.1$ Hz); ^{13}C NMR ($CDCl_3$, 100 MHz): δ 170.6 (C), 166.0 (C), 155.3 (C), 146.2 (C), 136.4 (C), 136.0 (CH), 129.3 (CH, 2×), 129.2 (CH, 2×), 128.8 (CH, 2×), 128.6 (CH, 2×), 127.1 (CH), 126.9 (CH), 121.5 (CH), 80.3 (C), 60.4 (CH_2), 56.0 (CH), 50.6 (CH), 40.4 (CH_2), 38.4 (CH_2), 28.2 (CH_3, 3×), 14.6 (CH_3); FAB-MS 467.57 (M^++H); HRMS calcd for $C_{27}H_{35}N_2O_5$, 467.5771 (M^++H); found, 467.5775.

4.2.5. Dipeptidomimetic α,β-unsaturated esters 18a–e. The Phe-Phe dipeptide α,β-unsaturated ester **17** (235 mg, 0.5 mmol) was treated with HCl in 1,4-dioxane, by a procedure similar to that for **14**, to give the corresponding aminium salt, which was then subjected to coupling reactions with appropriate (substituted) cinnamic acids (0.55 mmol) in DMF (10 mL) by promotion of HBTU (0.6 mmol) and *i*-Pr_2NEt (2.5 mmol), by a procedure similar to that for **1a**, to afford the dipeptide conjugated esters **18a**–**e** (69–83% yields).

4.2.5.1. Ethyl 5-phenyl-4-[2-(4-phenylcinnamyl)amino-1-oxo-3-phenyl]propylamino-2-pentenoate (18a). Colorless solid; mp 220–223 °C; TLC (CH_3OH/CH_2Cl_2, 1:19) $R_f = 0.45$; IR (KBr) 3211, 1709, 1629, 1521, 1259 cm^{-1}; ^1H NMR (DMSO-d_6, 400 MHz): δ 8.36 (2H, d, $J = 8.2$ Hz), 7.73–7.69 (4H, m), 7.63 (2H, d, $J = 8.2$ Hz), 7.46–7.42 (4H, m), 7.22–7.15 (10H, m), 6.78 (1H, dd, $J = 15.7$, 5.2 Hz), 6.75 (1H, d, $J = 15.7$ Hz), 5.67 (1H, d, $J = 15.7$ Hz), 4.71–4.65 (2H, m), 4.09 (2H, q, $J = 7.1$ Hz), 2.97–2.77 (4H, m), 1.19 (3H, t, $J = 7.1$ Hz); ^{13}C NMR (DMSO-d_6, 100 MHz): δ 171.0 (C), 165.9 (C), 165.1 (C), 148.5 (C), 141.4 (C), 139.8 (C), 138.9 (C), 138.1 (C), 138.0 (CH), 134.4 (CH), 129.7 (CH, 2×), 129.6 (CH, 2×), 129.5 (CH, 2×), 128.6 (CH, 2×), 128.5 (CH, 2×), 128.3 (CH, 2×), 127.6 (CH, 2×), 127.1 (CH, 2×), 126.8 (CH, 2×), 126.7 (CH), 122.4 (CH), 120.7 (CH), 60.4 (CH_2), 54.9 (CH), 51.4 (CH), 38.4 (CH_2, 2×), 14.6 (CH_3); FAB-MS *m/z* 573.28 (M^++H); HRMS calcd for $C_{37}H_{37}N_2O_4$, 573.2753 (M^++H); found, 573.2755. Anal. calcd for $C_{37}H_{36}N_2O_4$: C 77.60, H 6.34, N 4.89. Found: C 77.58, H 6.34, N 4.90.

4.2.5.2. Ethyl 4-[2-(4-nitrocinnamyl)amino-1-oxo-3-phenyl]propylamino-5-phenyl-2-pentenoate (18b). Colorless solid; mp 247–250 °C; TLC (EtOAc/hexane, 1:1) $R_f = 0.27$; IR (KBr) 3291, 1711, 1637, 1533, 1421, 1259 cm^{-1}; ^1H NMR (DMSO-d_6, 400 MHz): δ 8.49 (1H, d, $J = 8.5$ Hz), 8.38 (1H, d, $J = 8.5$ Hz), 8.25 (2H, d, $J = 8.7$ Hz), 7.80 (2H, d, $J = 8.7$ Hz), 7.49 (1H, d, $J = 15.8$ Hz), 7.29–7.14 (10H, m), 6.88 (1H, d, $J = 15.8$ Hz), 6.78 (1H, dd, $J = 15.8$, 5.2 Hz), 5.66 (1H, d, $J = 15.8$ Hz), 4.67–4.63 (2H, m), 4.09 (2H, q, $J = 7.1$ Hz), 2.96–2.65 (4H, m), 1.19 (3H, t, $J = 7.1$ Hz); ^{13}C NMR (DMSO-d_6, 100 MHz): δ 171.8 (C), 165.9 (C), 164.3 (C), 148.5 (C), 147.9 (C), 141.9 (C), 138.1 (C), 137.9 (CH), 137.1 (CH), 129.7 (CH), 129.5 (CH), 129.0 (CH), 128.6 (CH, 2×), 128.5 (CH, 2×), 126.8 (CH, 2×), 126.7 (CH, 2×), 126.6 (CH, 2×), 124.6 (CH, 2×), 120.1 (CH), 60.4 (CH_2), 54.7 (CH), 51.4 (CH), 39.3 (CH_2), 31.2 (CH_2), 14.6 (CH_3); FAB-MS *m/z* 542.23 (M^++H); HRMS calcd for $C_{31}H_{32}N_3N_3O_6$, 542.2291 (M^++H); found, 542.2289. Anal. calcd for $C_{31}H_{31}N_3O_6$: C 68.75, H 5.77, N 7.76. Found: C 68.77, H 5.56, N 7.76.

4.2.5.3. Ethyl 4-{2-[4-((dimethylamino)cinnaniyl]-amino-1-oxo-3-phenyl}propylamino-5-phenyl-2-pentenoate (18c). Colorless solid; mp 225–227 °C; TLC (EtOAc/hexane, 1:1) $R_f = 0.24$; IR (KBr) 3213, 1707, 1521, 1459, 1255 cm^{-1}; ^1H NMR (DMSO-d_6, 400 MHz): δ 8.32 (1H, d, $J = 8.2$ Hz), 8.16 (1H, d, $J = 8.2$ Hz), 7.36 (2H, d, $J = 8.6$ Hz), 7.29–7.14 (11H, m), 6.79 (1H, dd, $J = 15.8$, 5.1 Hz), 6.70 (2H, d, $J = 8.6$ Hz), 6.41 (1H, d, $J = 15.7$ Hz), 5.66 (1H, d, $J = 15.7$ Hz), 4.65–4.60 (2H, m), 4.09 (2H, q, $J = 7.1$ Hz), 2.94 (6H, s), 2.90–2.64 (4H, m), 1.18 (3H, t, $J = 7.1$ Hz); ^{13}C NMR (DMSO-d_6, 100 MHz): δ 171.2 (C), 166.0 (C), 165.9 (C), 151.5 (C), 148.6 (C), 139.8 (C), 138.2 (C), 129.7 (CH, 2×), 129.5 (CH, 2×), 129.3 (CH, 2×), 128.6 (CH, 2×), 128.5 (CH, 2×), 126.7 (CH, 2×), 122.7 (CH), 126.8 (CH, 2×), 120.6 (CH), 116.8 (CH), 112.4 (CH), 60.4 (CH_2), 54.6 (CH), 51.4 (CH), 40.5 (CH_2, 2×), 38.4 (CH_2, 2×), 14.6 (CH_3); FAB-MS *m/z* 540.06 (M^++H); HRMS calcd for $C_{33}H_{38}N_3O_4$, 540.0641 (M^++H); found, 540.0639. Anal. calcd for $C_{33}H_{37}N_3O_4$: C 73.44, H 6.91, N 7.79. Found: C 73.47, H 6.93, N 7.78.

4.2.5.4. Ethyl 4-[2-(2,4-dimethoxycinnamyl)amino-1-oxo-3-phenyl]propylamino-5-phenyl-2-pentenoate (18d). Colorless solid; mp 203–205 °C; TLC (EtOAc/hexane, 1:1) $R_f = 0.27$; IR (KBr) 3276, 2932, 1723, 1648, 1536, 1270, 1033 cm^{-1}; ^1H NMR ($CDCl_3$, 400 MHz): δ 7.77 (1H, d, $J = 15.7$ Hz), 7.40 (2H, d, $J = 8.5$ Hz), 7.30–7.14 (7H, m), 7.06 (2H, d, $J = 8.5$ Hz), 6.80 (1H, dd, $J = 15.7$, 5.2 Hz), 6.50 (1H, d, $J = 8.5$ Hz), 6.47 (1H, s), 6.38 (1H, d, $J = 15.7$ Hz), 6.37 (1H, br s), 6.05 (1H, br s), 5.61 (1H, d, $J = 15.7$ Hz), 4.85–4.76 (2H, m), 4.18 (2H, q, $J = 7.0$ Hz), 3.88 (3H, s), 3.85 (3H, s), 3.12–3.06 (2H, m), 2.85–2.76 (2H, m), 1.30 (3H, t, $J = 7.0$ Hz); ^{13}C NMR ($CDCl_3$, 100 MHz): δ 170.6 (C), 166.9 (C), 166.1 (C), 162.4 (C), 159.8 (C), 146.3 (CH), 137.3 (C), 136.5 (C), 136.3 (CH), 130.7 (CH), 129.3 (CH), 129.2 (CH, 2×), 128.7 (CH, 2×), 128.5 (CH, 2×), 127.0 (CH, 2×), 126.7 (CH), 121.4 (CH), 118.2 (C), 116.6 (CH), 105.0 (CH), 98.4 (CH), 60.4

(CH_2), 55.47 (CH_3), 55.41 (CH_3), 54.6 (CH), 51.1 (CH), 40.5 (CH_2), 38.4 (CH_2), 14.2 (CH_3); FAB-MS *m/z* 557.26 (M^++H); HRMS calcd for $C_{33}H_{37}N_2O_6$, 557.2651 (M^++H); found, 557.2656. Anal. calcd for $C_{33}H_{36}N_2O_6$: C 71.20, H 6.52, N 5.03. Found: C 71.17, H 6.54, N 5.03.

4.2.5.5. Ethyl 4-{2-[3,4-(methylenedioxy)cinnamyl]amino-l-oxo-3-phenyl}propylamino-5-phenyl-2-pentenoate (18e). Colorless solid; mp 192–194 °C; TLC (EtOAc/hexane, 1:1) R_f = 0.33; IR (KBr) 3297, 1726, 1666, 1547, 1448, 1249 cm^{-1}; ^1H NMR (DMSO-d_6, 400 MHz): δ 8.32 (1H, d, J = 8.3 Hz), 8.18 (1H, d, J = 8.4 Hz), 7.32–7.10 (12H, m), 7.04 (1H, d, J = 8.0 Hz), 6.93 (1H, d, J = 8.0 Hz), 6.78 (1H, dd, J = 15.7, 5.2 Hz), 6.53 (1H, d, J = 15.7 Hz), 6.05 (2 H, s), 5.65 (1H, d, J = 15.7 Hz), 4.67–4.63 (2 H, m), 4.09 (2 H, q, J = 7.0 Hz), 2.93–2.75 (4H, m), 1.19 (3H, t, J = 7.0 Hz); ^{13}C NMR (DMSO-d_6, 100 MHz): δ 171.0 (C), 165.9 (C), 165.3 (C), 148.9 (C), 148.5 (C), 148.4 (C), 139.2 (C), 138.8 (C), 138.1 (CH), 129.7 (CH), 129.5 (CH, 2×), 128.7 (CH), 128.6 (CH, 2×), 128.5 (CH, 2×), 126.8 (CH, 2×), 126.7 (CH), 123.7 (CH), 120.7 (CH), 120.4 (CH), 109.0 (CH), 106.2 (CH), 101.9 (CH_2), 60.4 (CH_2), 54.6 (CH), 51.4 (CH), 38.4 (CH_2, 2×), 14.6 (CH_3); FAB-MS *m/z* 541.23 (M^++H); HRMS calcd for $C_{32}H_{33}N_2O_6$, 541.2338 (M^++H); found, 541.2341. Anal. calcd for $C_{32}H_{32}N_2O_6$: C 71.09, H 5.97, N 5.18. Found: C 71.11, H 5.99, N 5.17.

4.2.6. Ethyl 4-{2-[3,4-(methylenedioxy)cinnamyl]amino-1-oxo-3-phenyl} propylamino-5-(2-oxo-3-pyrrolidyl)-2-pentenoate (19). Condensation of L-Phe-OMe with 3,4-(methylenedioxy)cinnamic acid in the presence of EDCI, HOBt, and 4-methylmorpholine, followed by hydrolysis (LiOH, MeOH/H_2O), afforded *N*-[3,4-(methylenedioxy)cinnamyl]phenylalanine in 64% yield. This product was reacted with the aminium salt **8** (HBTU, *i*-Pr_2NEt, DMF, 0 °C to rt, 7 h), by a procedure similar to that for **18a**–**e**, to give the title compound **19** in 57% yield.

Compound **19**: white solid; mp 103–105 °C; TLC (MeOH/CH_2Cl_2, 1:99) R_f = 0.24; IR (KBr) 3283, 2919, 1683, 1447, 1241 cm^{-1}; ^1H NMR ($CDCl_3$, 400 MHz): δ 7.81 (1H, d, J = 7.0 Hz), 7.50 (1H, d, J = 15.5 Hz), 7.29–7.20 (4H, m), 7.00–6.94 (2H, m), 6.79–6.67 (3H, m), 6.31–6.26 (2H, m), 5.99 (2H, s), 5.75 (1H, d, J = 15.5 Hz), 5.10–5.00 (1H, m), 4.57–4.40 (1H, m), 4.18 (2H, q, J = 7.1 Hz), 3.31–3.19 (3H, m), 3.08–3.06 (1H, m), 2.23–2.12 (2H, m), 2.10–1.81 (2H, m), 1.80–1.40 (2H, m), 1.30 (3H, t, J = 7.0 Hz); ^{13}C NMR ($CDCl_3$, 100 MHz): δ 171.2 (C), 166.2 (C), 165.8 (C), 165.7 (C), 149.2 (C), 148.2 (C), 146.8 (CH), 141.3 (C), 136.5 (CH), 129.7 (C), 129.1 (CH), 128.5 (CH, 2×), 126.9 (CH, 2×), 124.1 (CH), 121.2 (CH), 118.3 (CH), 108.5 (CH), 106.4 (CH), 101.4 (CH_2), 60.5 (CH_2), 54.8 (CH), 54.3 (CH), 49.5 (CH), 40.7 (CH_2), 38.9 (CH_2), 34.8 (CH_2), 29.7 (CH_2), 14.2 (CH_3); FAB-MS 548.24 (M^++H); HRMS calcd for $C_{30}H_{34}N_3O_7$, 548.2397 (M^++H); found, 548.2399.

4.2.7. Ethyl 4-[*N*-(3,4-methylenedioxy)cinnamyl-valinyl-phenylalanyl]-5-phenyl-2-pentenoate (20). By a procedure similar to that for **19**, condensation of L-Val-OMe with 3,4-methylenedioxycinnamic acid gave *N*-(3,4-methylenedioxy)cinnamyl-valine, which was subjected to amidation with the amine derived from **17** to give compound 20 in 73% yield.

Compound **20**: white solid; mp 207–209 °C; TLC (MeOH/CH_2Cl_2, 1:19) R_f = 0.32; IR (KBr) 3284, 1678, 1437, 1255 cm^{-1}; ^1H NMR (DMSO-d_6, 400 MHz): δ 8.13 (2H, d, J = 7.1 Hz), 7.93 (1H, d, J = 7.1 Hz), 7.35–6.93 (14H, m), 6.93–6.60 (2H, m), 6.05 (2H, s), 5.62 (1H, d, J = 15.5 Hz), 4.66–4.60 (1H, m), 4.50–4.47 (1H, m), 4.24–4.21 (1H, m), 4.09 (2H, q, J = 7.1 Hz), 2.91–2.65 (4H, m), 2.02–1.87 (1H, m), 1.21–1.15 (9H, m); ^{13}C NMR (DMSO-d_6, 100 MHz): δ 171.2 (C), 170.7 (C), 165.9 (C), 165.8 (C), 148.9 (C), 148.4 (C), 148.3 (CH), 139.2 (C), 138.1 (C), 137.9 (CH), 129.8 (C), 129.6 (CH, 2×), 129.5 (CH, 2×), 128.7 (CH, 2×), 128.6 (CH, 2×), 128.5 (CH), 126.7 (CH), 123.7 (CH), 120.7 (CH), 120.6 (CH), 109.1 (CH), 106.5 (CH), 101.9 (CH_2), 60.2 (CH_2), 58.4 (CH), 54.6 (CH), 51.2 (CH), 40.6 (CH_2), 39.3 (CH_2), 30.9 (CH), 19.6 (CH_3), 19.4 (CH_3), 14.3 (CH_3); FAB-MS 640.30 (M^++H); HRMS calcd for $C_{37}H_{42}N_3O_7$, 640.3023 (M^++H); found, 640.3027.

4.2.8. *N*,*N*′-Bis-[2-(1-benzyl-3-ethoxycarbonyl)propenyl]1,4-butanediamide (21a). Ethyl (2*E*,4*S*)-4-(*tert*-butoxycarbonyl)amino-5-phenyl-2-pentenoate[23] was treated with HCl in 1,4-dioxane to remove the Boc group, and the resulting amine was reacted with succinic acid in the presence of EDCI, HOBt, and 4-methylmorpholine, by a procedure similar to that for **17**, to give **21a** in 80% yield.

Compound **21a**: TLC (EtOAc/hexane, 1:4) R_f = 0.21; IR (KBr) 3304, 3065, 2998, 1731, 1646, 1547, 1308, 1189 cm^{-1}; ^1H NMR ($CDCl_3$, 300 MHz): δ 7.27–7.10 (10H, m), 6.86 (2H, dd, J = 13.6, 8.0 Hz), 6.48 (2H, d, J = 8.5 Hz), 5.81 (2H, dd, J = 13.6, 4.2 Hz), 4.87 (2H, dd, J = 13.2, 6.1 Hz), 4.10 (4H, q, J = 7.6 Hz), 2.93–2.77 (4H, m), 2.46 (4H, s), 1.23 (6H, t, J = 7.6 Hz); ^{13}C NMR ($CDCl_3$, 75 MHz): δ 171.5 (C, 2×), 166.0 (C, 2×), 146.7 (CH, 2×), 136.4 (C, 2×), 129.3 (CH, 4×), 128.5 (CH, 4×), 126.8 (CH, 2×), 121.3 (CH, 2×), 60.6 (CH, 2×), 51.2 (CH_2, 2×), 40.3 (CH_2, 2×), 31.4 (CH_2, 2×), 14.1 (CH_3, 2×); FAB-MS *m/z* 521.28 (M^++H); HRMS calcd for $C_{30}H_{37}N_2O_6$, 521.2652 (M^++H); found, 521.2655.

4.2.9. *N*,*N*′-Bis-[2-(1-benzyl-3-ethoxycarbonyl)propenyl]2-hydroxy-1,4-butanediamide (21b). Using (*S*)-malic acid in lieu of succinic acid, compound **21b** was prepared by a procedure similar to that for **21a.**

Compound **21b**: white solid; TLC (CH_3OH/CH_2Cl_2, 1:19) R_f = 0.23; IR (KBr) 3310, 3068, 1718, 1654, 1533, 1371, 1287, 1182 cm^{-1}; ^1H NMR ($CDCl_3$, 300 MHz): δ 7.29–7.07 (10H, m), 6.92–6.77 (2H, m), 5.83–5.77 (2H, m), 5.81 (1H, br s), 4.85–4.78 (2H, m), 4.22 (2H, d, J = 6.7 Hz), 4.17–4.08 (4H, m), 2.93–2.78 (4H, m), 2.86–2.56 (2H, m), 2.19 (1H, dd, J = 15.6, 8.6 Hz), 1.25–1.17 (6H, m); ^{13}C NMR ($CDCl_3$, 75 MHz): δ 171.9 (C), 171.5 (C), 165.9 (C, 2×), 146.2

(CH), 146.1 (CH), 136.2 (C), 136.1 (C), 129.35 (CH, 2×), 129.25 (CH, 2×), 128.6 (CH, 2×), 128.5 (CH, 2×), 126.96 (CH), 126.92 (CH), 121.6 (CH), 121.5 (CH), 69.03 (CH), 60.6 (CH), 60.5 (CH), 51.0 (CH_2), 50.6 (CH_2), 40.5 (CH_2), 40.2 (CH_2), 38.9 (CH), 14.1 (CH_3, 2×); FAB-MS *m*/*z* 537.3 (M^++H); HRMS calcd for $C_{30}H_{37}N_2O_7$, 537.2601 (M^++H); found, 537.2600.

4.2.10. *N*,*N*′-Bis-2-(1-benzyl-3-ethoxycarbonyl)propenyl]2,3-dihydroxy-1,4-butanediamide (21c). Using (2*R*,3*R*)-tartaric acid in lieu of succinic acid, compound **21c** was prepared by a procedure similar to that for **21a.**

Compound **21c**: TLC (CH_3OH/CH_2Cl_2, 1:19) R_f = 0.21; IR (neat) 3357, 2986, 2926, 1706, 1646, 1534, 1295, 1169 cm^{-1}; ^1H NMR ($CDCl_3$, 400 MHz): δ 7.32–7.25 (6H, m), 7.16 (4H, d, J = 8.3 Hz), 6.87 (2H, dd, J = 15.7, 4.3 Hz), 5.74 (2H, dd, J = 15.7, 2.0 Hz), 5.01–4.93 (4H, m), 4.17–4.12 (4H, m), 2.89–2.87 (8H, m), 1.23 (6H, t, J = 7.1 Hz); ^{13}C NMR ($CDCl_3$, 100 MHz): δ 166.1 (C, 2×), 162.7 (C, 2×), 146.4 (C, 2×), 136.2 (CH, 2×), 129.3 (CH, 4×), 128.6 (CH, 4×), 126.9 (CH, 2×), 121.3 (CH, 2×), 71.5 (CH, 2×), 60.5 (CH_2, 2×), 50.7 (CH, 2×), 40.3 (CH_2, 2×), 14.1 (CH, 2×).

4.3. Inhibition assay against the SARS-CoV 3CL protease

A fluorometric assay[19] was utilized to determine the inhibition constants of the prepared samples. Briefly, a fluorogenic peptide Dabcyl-KTSAVLQSGFRKME-Edans was used as the substrate; and the enhanced fluorescence due to cleavage of this substrate catalyzed by the protease was monitored at 538 nm with excitation at 355 nm. The IC_{50} value of individual sample was measured in a reaction mixture containing 50 nM of the SARS-CoV 3CL protease and 6 μM of the fluorogenic substrate in 20 mM Bis–Tris (pH 7.0). The enzyme stock solution was kept in 12 mM Tris–HCl (pH 7.5) containing 120 mM NaCl, 0.1 mM EDTA, and 1 mM DTT plus 7.5 mM β-ME before adding to the assay solution. The K_i measurements were performed at two fixed inhibitor concentrations and various substrate concentrations.

4.4. Cell-based assay for the anti-SARS agents

Vero E6 cells (2×10^4/well) were cultured in a 96-well plate in FBS DMEM supplemented with 10% FBS. The culture medium was removed after 1-day incubation when the cells reached 80–90% confluence. A solution of 100 μL DMEM with 2% FBS containing the compound to be tested, was placed in three wells. Three wells containing cells in DMEM, with 2% FBS were used as the CPE-positive control. Cells were incubated in a CO_2 incubator at 37 °C for 2 h, inoculated with SARS-CoV (H.K.) at a dose of 100 $TCID_{50}$/well, and the cytopathic morphology of the cells was examined using an inverted microscope 72 h after infection.

4.5. Cytotoxicity study

Vero E6 cells were grown in DMEM supplemented with L-glutamine, nonessential amino acids, and 10% FBS. The cells were cultured in 75 cm^2 flasks and incubated in a humidified 5% CO_2 incubator at 37 °C. Cells were later seeded at 7×10^4 cells/mL onto a 96-well plate and left overnight before cytotoxicity study. MTS assay was performed using Cell Titer 96 nonRadioactive Cell Proliferation Assay Kits (Promega Co., Madison, WI, USA) to determine the population of living cells.[23] This assay measures the amount of Formazan produced by metabolic conversion of Owen's reagent, [3-(4,5-dimethylthiazol-2-yl)-5-(3-carboxymethoxyphenyl)-2-(4-sulfophenyl)-2*H*-tetrazolium, inner salt; MTS], by a dehydrogenase present in the mitochondria of metabolically active cells and is directly proportional to the number of living cells. Briefly, after the incubations with the tested compounds at varied concentrations for 2 days, the culture medium was replaced with MTS/PMS in DMEM. After incubation for 2 h at 37 °C, the absorbance of the samples was measured with a plate reader at 490 nm. Data are expressed as percentage of control cells (as 100%) cultured in the absence of any tested compounds.

4.6. ELISA of anti-SARS agents

At the conclusion of the incubation, the SARS-virus-infected Vero E6 cells were rinsed with PBS, fixed in an ice-cold methanol/acetone (1:1) solution for 3 min at room temperature, and rinsed three times with PBS. The cells were blocked with 3% skimmed milk in PBS for 30 min at room temperature, and then incubated for 1 h at 37 °C with 1:2000 diluted monoclonal antibody (ascetic fluid) to the spike protein of SARS-CoV. All samples were washed with three changes of PBS-T buffer and twice with fresh changes of PBS buffer at room temperature, followed by incubation with HRP-labeled goat anti-mouse IgG for 30 min at room temperature. The plates were rinsed with PBS containing 0.05% Tween 20 between incubations. A substrate solution containing *O*-phenylenediamine dihydrochloride, citrate buffer (pH 5.0), and hydrogen peroxide was added to each well. The plates were covered and gently shaken at room temperature for 10 min. The reaction was stopped by the addition of sulfuric acid (3 N) and the plates were read immediately at 492 nm. The EC_{50} value for each tested agent was extrapolated from the linear regression plot of the agent concentration versus OD_{492}.

4.7. Western blot analysis of anti-SARS agents

SARS-CoV-infected Vero E6 cells were treated with compounds at varied concentrations for 24 or 48 h then lysed in a lysis buffer for 3 min. The cell debris was spun down and all cell lysates were harvested for electrophoresis and Western blotting assay with SDS–PAGE and a Hybond-C Extra membrane (Amersham Pharmacia). The resulting membrane was blocked in 3% skimmed milk in PBS for 30 min at room temperature, and then treated with 1:1000 diluted antispike protein monoclonal antibody (ChemiconMAb 1501) for 1 h at room temperature. The membrane was rinsed by using two changes of PBS-T buffer, and then washed once for 15 min and twice for 5 min each with fresh PBS buffer at room temperature, followed by treatment with horse-

radish peroxidase-labeled goat anti-mouse IgG for 30 min and 1:2000 dilution for 1 h. The membrane was washed as above, and the mixed enhanced chemiluminescence detection reagent was added to the protein side of the membrane. The blot was placed with the protein side up, in the film cassette, to visualize the level of protein expression.

4.8. Computer modeling

Docking experiments were conducted by using Autodock 3.0.5 with a Lamarckian Genetic Algorithm (LGA).[27] The crystal structure (PDB code 1c145a) for the complex of a mutated (C145A) SARS-CoV 3CL protease with a hexapeptide substrate of Ser-Gly-Val-Thr-Phe-Gln was refined using Cys at residue 145 and only the apo chain B of the dimer in this simulation. The structures of inhibitory compounds were built in CAChe (Fujitsu, Japan) and refined by performing an optimized geometry calculation in Mechanics using augmented MM2 parameters and stored in PDB format. MGLTOOLS (MGL, Scripps Institute) was used for structure preparation and parameter creation to meet the input requirements of Autodock. Briefly, essential hydrogen atoms were added to the structure model of $3CL^{pro}$ followed by assigning Kollman united atom charges and solvation parameters. Compound molecules were assigned Gasteiger–Marsili charges,[28] merge nonpolar H atoms, and defined torsions. Autogrid tool in Autodock 3.0.5 was applied to compute energy grids ($60 \times 60 \times 70$ in *xyz* directions with 0.375 Å spacing) of various types of compound atoms. These grip maps were centered at the active site. During docking experiments, each compound was kept flexible (except for their rings and amide bonds) and the protein was rigid. Solis and Wets' local search method with LGA was applied to generate available conformations of compound structures within the active site. The conformational search was conducted utilizing 0.2 Å quaternion and 2° torsion steps. For each compound structure, 5×10^6 energy was evaluated and 80 poses were selected from 5×10^5 generations per run. Plausible docking modes were elected by collecting binding free energies, clustering all simulated poses structures within 2.0 Å root mean square deviations, and selecting the most abundant cluster with highest affinity energy. The conserved hydrogen bond interactions with Glu166 and Gln189, which observed in crystal complex, were considered as the additional factors when electing the binding mode. Pictures of the final simulated docking modes were generated in MGLTOOLS.

Acknowledgment

We thank National Science Council for financial support.

References and notes

1. (a) Ksiazek, T. G.; Erdman, D.; Goldsmith, C. S.; Zaki, S. R.; Peret, T.; Emery, S.; Tong, S.; Urbani, C.; Comer, J. A.; Lim, W., et al. *N. Engl. J. Med.* **2003**, *348*, 1953–1966; (b) Drosten, C.; Günther, S.; Preiser, W.; van der Werf, S.; Brodt, H.-R.; Becker, S.; Rabenau, H.; Panning, M.; Kolesnikova, L.; Fouchier, R. A. M., et al. *N. Engl. J. Med.* **2003**, *348*, 1967–1976; (c) Peiris, J. S. M.; Lai, S. T.; Poon, L. L. M.; Guan, Y.; Yam, L. Y. C.; Lim, W.; Nicholls, J.; Yee, W. K. S.; Yan, W. W.; Cheung, M. T., et al. *Lancet* **2003**, *361*, 1319–1325.
2. World Helth Organization, Communicable Disease Surveillance & Response, website: http://www.who.int/csr/sars/archive/2003_05_07a/en and http://www.who.int/csr/sars/country/en/country2003_08_15.pdf. Summary table of SARS cases by country (1 November, 2002, to 7 August, 2003).
3. He, J.-F.; Peng, G.-W.; Min, J.; Yu, D.-W.; Liang, W.-L.; Zhang, S.-Y.; Xu, R.-H.; Zheng, H.-Y.; Wu, X.-W.; Xu, J., et al. *Science* **2004**, *303*, 1666–1669.
4. (a) Rota, P. A.; Oberste, M. S.; Monroe, S. S.; Nix, W. A.; Campagnoli, R.; Icenogle, J. P.; Penaranda, S.; Bankamp, B.; Maher, K.; Chen, M.-H. *Science* **2003**, *300*, 1394–1399; (b) Marra, M. A.; Jones, S. J. M.; Astell, C. R.; Holt, R. A.; Brooks-Wilson, A.; Butterfield, Y. S. N.; Khattra, J.; Asano, J. K.; Barber, S. A.; Chan, S. Y., et al. *Science* **2003**, *300*, 1399–1404; (c) Ruan, Y. J.; Wei, C. L.; Ee, L. A.; Vega, V. B.; Thoreau, H.; Yun, S. T. S.; Chia, J. M.; Ng, P.; Chiu, K. P.; Lim, L., et al. *Lancet* **2003**, *361*, 1779–1785.
5. (a) Anand, K.; Ziebuhr, J.; Wadhwani, P.; Mesters, J. R.; Hilgenfeld, R. *Science* **2003**, *300*, 1763–1767; (b) Yang, H.; Yang, M.; Ding, Y.; Liu, Y.; Lou, Z.; Zhou, Z.; Sun, L.; Mo, L.; Ye, S.; Pang, H.; Gao, G. F.; Anand, K.; Bartlam, M.; Hilgenfeld, R.; Rao, Z. *Proc. Natl. Acad. Sci. U.S.A.* **2003**, *100*, 13190–13195; (c) Chou, K.; Wei, D.; Zhong, W. *Biochem. Biophys. Res. Commun.* **2003**, *308*, 148–151.
6. (a) Fan, K.; Wei, P.; Feng, Q.; Chen, S.; Huang, C.; Ma, L.; Lai, B.; Pei, J.; Liu, Y.; Chen, J.; Lai, L. *J. Biol. Chem.* **2004**, *279*, 1637–1642; (b) Huang, C.; Wei, P.; Fan, K.; Liu, Y.; Lai, L. *Biochemistry* **2004**, *43*, 4568–4574; (c) Du, Q.-S.; Wang, S.-Q.; Zhu, Y.; Wei, D.-Q.; Guo, H.; Sirois, S.; Chou, K.-C. *Peptides* **2004**, *25*, 1857–1864.
7. Wu, C.-Y.; Jan, J.-T.; Ma, H.-H.; Kuo, C.-J.; Juan, H.-F.; Cheng, Y.-S. E.; Hsu, H.-H.; Huang, H.-C.; Wu, D.; Brik, A.; Liang, F.-S.; Liu, R.-S.; Fang, J.-M.; Chen, S.-T.; Liang, P.-H.; Wong, C.-H. *Proc. Natl. Acad. Sci. U.S.A.* **2004**, *101*, 10012–10017.
8. Hsu, J. T.-A.; Kuo, C.-J.; Hsieh, H.-P.; Wang, Y.-C.; Huang, K.-K.; Lina, C. P.-C.; Huang, P.-F.; Chen, X.; Liang, P.-H. *FEBS Lett.* **2004**, *574*, 116–120.
9. Bacha, U.; Barrila, J.; Velazquez-Campoy, A.; Leavitt, S. A.; Freire, E. *Biochemsitry* **2004**, *43*, 4906–4912.
10. Kao, R. Y.; Tsui, W. H. W.; Lee, T. S. W.; Tanner, J. A.; Watt, R. M.; Huang, J.-D.; Hu, L.; Chen, G.; Chen, Z.; Zhang, L.; He, T.; Chan, K.-H.; Tse, H.; To, A. P. C.; Ng, L. W. Y.; Wong, B. C. W.; Tsoi, H.-W.; Yang, D.; Ho, D. D.; Yuen, K.-Y. *Chem. Biol.* **2004**, *11*, 1293–1299.
11. Blanchard, J. E.; Elowe, N. H.; Huitema, C.; Fortin, P. D.; Cechetto, J. D.; Eltis, L. D.; Brown, E. D. *Chem. Biol.* **2004**, *11*, 1445–1453.
12. Jain, R. P.; Pettersson, H. I.; Zhang, J.; Aull, K. D.; Fortin, P. D.; Huitema, C.; Eltis, L. D.; Parrish, J. C.; James, M. N. G.; Wishart, D. S.; Vederas, J. C. *J. Med. Chem.* **2004**, *47*, 6113–6116.
13. (a) Dragovich, P. S.; Prins, T. J.; Zhou, R.; Webber, S. E.; Marakovits, J. T.; Fuhrman, S. A.; Patick, A. K.; Matthews, D. A.; Lee, C. A.; Ford, C. E.; Burke, B. J.; Rejto, P. A.; Hendrickson, T. F.; Tuntland, T.; Brown, E. L.; Meador, J. W., III; Ferre, R. A.; Harr, J. E. V.; Kosa, M. B.; Worland, S. T. *J. Med. Chem.* **1999**, *42*, 1213–1224; (b) Patick, A. K.; Binford, S. L.; Brothers, M. A.; Jackson, R. L.; Ford, C. E.;

Diem, M. D., et al. *Antimicrob. Agents Chemother.* **1999**, *43*, 2444–2450; (c) Matthews, D. A.; Dragovich, P. S.; Webber, S. E.; Fuhrman, S. A.; Patick, A. K.; Zalman, L. S.; Hendrickson, T. F.; Love, R. A.; Prins, T. J.; Marakovits, J. T.; Zhou, R.; Tikhe, J.; Ford, C. E.; Meador, J. W.; Ferre, R. A.; Brown, E. L.; Binford, S. L.; Brothers, M. A.; Delisle, D. M.; Worland, S. T. *Proc. Natl. Acad. Sci. U.S.A.* **1999**, *96*, 11000–11007.

14. (a) Kräusslich, H. G.; Wimmer, E. *Annu. Rev. Biochem.* **1988**, *57*, 701–754; (b) Kay, J.; Dunn, B. M. *Biochem. Biophys. Acta* **1990**, *1048*, 1–18; (c) Lawson, M. A.; Semler, B. L. *Curr. Top. Microbiol. Immunol.* **1990**, *161*, 49–87.
15. Sirois, S.; Wei, D.-Q.; Du, Q.; Chou, K.-C. *J. Chem. Inf. Comput. Sci.* **2004**, *44*, 1111–1122.
16. (a) Tian, Q.; Nayyar, N. K.; Babu, S.; Tao, J.; Moran, T. J.; Dagnino, R.; Mitchell, L. J.; Remarchuk, T. P.; Melnick, M. J.; Bender, S. L. U.S. Pat. Appl. Publ. **2002**.(b) Tian, Q.; Nayyar, N. K.; Babu, S.; Chen, L.; Tao, J.; Lee, S.; Tibbetts, A.; Moran, T.; Liou, J.; Guo, M.; Kennedy, T. P. *Tetrahedron Lett.* **2001**, *42*, 6807–6809.
17. (a) Larchevêque, M.; Petit, Y. *Tetrahedron Lett.* **1987**, *28*, 1993–1996; (b) Pègorier, L.; Petit, Y.; Larchevêque, M. *Synthesis* **1994**, 1403–1405.
18. Street, L. J.; Sternfeld, F.; Jelley, R. A.; Reeve, A. J.; Carling, R. W.; Moore, K. W.; McKernan, R. M.; Bindi Sohal, B.; Cook, S.; Pike, A.; Dawson, G. R.; Bromidge, F. A.; Wafford, K. A.; Seabrook, G. R.; Thompson, S. A.; Marshall, G.; Pillai, G. V.; Castro, J. L.; Atack, J. R.; MacLeod, A. M. *J. Med. Chem.* **2004**, *47*, 3642–3657.
19. Kuo, C.-J.; Chi, Y.-H.; Hsu, T.-A.; Liang, P.-H. *Biochem. Biophys. Res. Commun.* **2004**, *318*, 862–867.
20. An interview mentions that AG7088 may be inactive against the SARS-CoV 3CL protease. See: Clarke, T. *Nature* **2003**, 423 (May 15). http://www.nature.com/nature/focus/SARS/index.html.
21. Hsu, M.-F.; Kuo, C.-J.; Chang, K.-T.; Chang, H.-C.; Chou, C.-C.; Ko, T.-P.; Shr, H.-L.; Chang, G.-G.; Wu, Y.-T.; Andrew Wang, H.-J.; Liang, P.-H. *J. Biol. Chem.* **2005**, in press.
22. (a) Wu, C.-Y.; Chang, C.-F.; Chen, J. S.-Y.; Wong, C.-H.; Lin, C.-H. *Angew. Chem., Int. Ed.* **2003**, *42*, 4661–4664; (b) Chang, C.-F.; Ho, C.-W.; Wu, C.-Y.; Chao, T.-A.; Wong, C.-H.; Lin, C.-H. *Chem. Biol.* **2004**, *11*, 1301–1306.
23. Ohba, T.; Ikeda, E.; Wakayama, J.; Takei, H. *Bioorg. Med. Chem. Lett.* **1996**, *6*, 219–224.
24. Buttke, T. M.; McCubrey, J. A.; Owen, T. C. *J. Immunol. Methods* **1993**, *157*, 233–240.
25. Kohl, N. E.; Emini, E. A.; Schleif, W. A.; Davis, L. J.; Heimbach, J. C.; Dixon, R. A. F.; Scolnick, E. M.; Sigal, I. S. *Proc. Natl. Acad. Sci. U.S.A.* **1988**, *85*, 4686–4690.
26. Kraüsslich, H.-G. *Proc. Natl. Acad. Sci. U.S.A.* **1991**, *88*, 3213–3217.
27. Morris, G. M.; Goodsell, D. S.; Halliday, R. S.; Heuy, R.; Hart, W. E.; Belew, R. K.; Olson, A. J. *J. Comput. Chem.* **1998**, *19*, 1639–1662.
28. Gasteiger, J.; Marsili, M. *Tetrahedron* **1980**, *36*, 3219–3288.